Proceedings of the 6th International Congress of Chinese Mathematicians
ALM 37, pp. 565–584

Wetting and Spreading of Drops on Rough Surfaces

Yi Shi and Xiao-Ping Wang

Abstract

In this paper, the quasi-static motion of two-phase flows on topologically rough surfaces is studied. By considering the Gibbs free energy of the system, we first consider the Cassie and Wenzel states transition on rough surfaces. It has been found that the crucial conditions for the two different states depend on the equilibrium contact angle, the droplet size and its initial position. Then the contact angle hysteresis on roughness induced superhydrophobic surfaces is investigated. We found that there are multiple local minimums and one global minimum for the Gibbs free energy landscape, which can reveal the mechanism of the stick-slip phenomena. When the scale of roughness becomes smaller, the stick-slip becomes weaker and the apparent contact angle will get closer to the Cassie-Baxter's angle. Numerical simulations of a phase field model agree very well with the analytical results.

Mathematics Subject Classification: 35, 65, 76.

Keywords and Phrases: Wetting, contact angle, generalized Navier boundary condition.

1 Introduction

The study of how liquid droplets move across a solid surface is of critical importance for many applications, ranging from micro-fluidic devices to fuel cells and ink-jet printing. When a droplet is put on a flat and chemically homogeneous surface, the equilibrium contact angle θ_s is given by the Young's equation,

$$\gamma_{LV} \cos\theta_s = \gamma_{SV} - \gamma_{SL}, \tag{1.1}$$

where γ_{LV}, γ_{SV} and γ_{SL} are the surface tensions of liquid-vapor, solid-vapor and solid-liquid interfaces, respectively. However, the situation of droplets spreading on topologically rough surfaces is quite different. On a topologically rough surface,

a droplet can attain two possible equilibrium states: it can appear either in the Cassie state, where the droplet sits suspended on top of posts with pockets of air beneath it, or in the Wenzel state, where the droplet penetrates into the grooves and wets the bottom substrate between the post. In the case of Cassie state, the apparent contact angle is usually given by

$$\cos\theta = \lambda\cos\theta_s - (1-\lambda), \tag{1.2}$$

where λ is the fraction of the solid-liquid interface below the drop, and in the Wenzel state, the apparent contact angle is usually given by

$$\cos\theta = r\cos\theta_s, \tag{1.3}$$

where r is the ratio between the real substrate area and its projection onto the horizontal plane. The equations (1.2) and (1.3) are called Cassie-Baxter's equation and Wenzel's equation respectively. Moreover, it has been found that the contact angle on such surfaces can take a range of values between two extremes: the advancing and receding contact angles. The advancing contact angle is measured for the droplet recently advances over the rough surface whereas the receding contact angle refers to the contact angle measured for the droplet recently retreats from the rough surface. The difference between the advancing and receding contact angles is called the contact angle hysteresis.

There have been many experimental and theoretical work on the topic of droplet spreading on topologically rough surfaces [18, 19, 20, 21, 22]. In [22], the authors studied the stick-slip motion of water droplets on striped surfaces experimentally. The transition between the collapsed and suspended states on a superhydrophobic surface is investigated in [11] both analytical and numerically. They concluded that the equilibrium state of the droplet depends on the intrinsic contact angle, the droplet size and its initial position. In [12, 13, 14], J. M. Yeomans et al. studied the contact angle hysteresis on chemically patterned and superhydrophobic surfaces using the lattice Boltzmann method. They pointed out that the advancing contact angle on such surfaces is 180° and the receding contact angle is the intrinsic contact angle of the surface.

In this paper, we first introduce a phase field model for two phase flows on rough surfaces. The model is derived form minimizing the total free energy, which includes the energy both in the bulk and on the boundary of the system. Then we study two interesting phenomena of droplets spreading on topologically rough surfaces. The first is the phenomena of Wenzel and Cassie states transition. By considering the Gibbs free energy of the system, we find there is a critical value for the equilibrium contact angle. For contact angle greater than the critical value, the droplet will always be static in Cassie state. When the contact angle is smaller than the critical value, the state of the droplet is determined by the droplet size and its initial positions. Numerical simulations of our phase field model can agree quantitatively well with the analytical results. The second is the phenomena of contact angle hysteresis on roughness induced superhydrophobic surfaces. We find that there are multiple local minimums and one global minimum for the Gibbs free energy landscape. Between two neighboring local minimums, there

may be an energy barrier, which reveals the mechanism for the stick-slip motion of the interface and the contact angle hysteresis on these surfaces. When the scale of roughness approaches to zero, we can show that the apparent contact angle should satisfy the Cassie-Baxter's equation. By the simulation of our phase field model, it can overcome some free energy barriers because of the diffusive interface thickness. This plays the role of energy fluctuation and is physically reasonable. Furthermore, by our simulations, when the size of roughness becomes smaller, the stick-slip becomes weaker and the apparent contact angle approaches to the Cassie-Baxter's angle, which also implies that the Cassie-Baxter's angle is the most stable contact angle when the droplet size is much larger than the size of roughness.

The remaining of this paper is organized as follows. In Section 2, we introduce the phase field model with its corresponding boundary conditions. Section 3 includes two parts: in Section 3.1, we describe the theoretical argument to predict the transition between Cassie and Wenzel states by considering the Gibbs free energy of the system, and then we present some numerical results using our phase field model. They are shown to be in good accordance. In Section 3.2, we first give the free energy landscape of the droplet on two dimensional roughness induced superhydrophobic surface, and then discuss it with the simulation results of the phase field model. The paper is concluded in Section 4.

2 The phase field model

The wetting phenomena of two phase flows on solid substrate can be described by the Ginzburg-Landau free energy theory. Using this theory, we can describe the total free energy of the form

$$F(\phi) = \int_\Omega \left(\frac{\epsilon}{2} |\nabla \phi|^2 + \frac{1}{\epsilon} f(\phi) \right) d\Omega + \int_{\partial\Omega} \gamma(\phi) dS, \tag{2.1}$$

where ϵ is a small parameter to characterize the interface thickness, ϕ is the order parameter, e.g. $\phi = 1$ represents liquid and $\phi = -1$ represents vapor. $f(\phi)$ is the bulk free energy density in Ω and is usually chosen to be a double well function

$$f(\phi) = \frac{1}{4}(1 - \phi^2)^2. \tag{2.2}$$

$\gamma(\phi)$ is the free energy density at the fluid-solid interface $\partial\Omega$ and is usually taken to be an interpolation between $\gamma_{SV} = \gamma(-1)$ and $\gamma_{SL} = \gamma(1)$ in the form of

$$\gamma(\phi) = \frac{\gamma_{SV} + \gamma_{SL}}{2} - \frac{\gamma_{SV} - \gamma_{SL}}{2} \sin\left(\frac{\pi}{2}\phi\right).$$

The equilibrium interface structure is obtained by minimizing the total free energy with fixed droplet size, which is the following constrained minimization problem

$$\min \ \{F(\phi)\}, \quad \text{s.t.} \int_\Omega \phi \ d\Omega = C_0. \tag{2.3}$$

Thus the Euler-Lagrange equation for the above constrained minimizing problem is

$$\begin{cases} -\epsilon\Delta\phi + \dfrac{1}{\epsilon}f'(\phi) = c, & \text{in } \Omega, \\ \epsilon\partial_n\phi + \dfrac{\partial\gamma}{\partial\phi} = 0, & \text{on } \partial\Omega, \end{cases} \tag{2.4}$$

subject to $\int_\Omega \phi \, d\Omega = C_0$.

The dynamics of the interface structure follows a relaxation dynamics both in the bulk and on the boundary and is described by the fourth order Cahn-Hilliard equation. By setting $\phi = \phi(t, x)$, the problem becomes the following gradient flow system

$$\begin{cases} \phi_t = M\Delta\mu, \quad \mu = -\epsilon\Delta\phi + \frac{1}{\epsilon}f'(\phi), & \text{in } \Omega, \\ \phi_t = -\Gamma\left(\epsilon\partial_n\phi + \dfrac{\partial\gamma}{\partial\phi}\right), \quad \frac{\partial\mu}{\partial n} = 0, & \text{on } \partial\Omega, \end{cases} \tag{2.5}$$

where M and Γ are positive phenomenological parameters, and μ is the chemical potential of the system.

By taking the incompressible hydrodynamics into consideration, the above equations can be coupled with the Navier-Stokes equations with the generalized Navier boundary conditions [1, 2, 3, 4],

$$\begin{cases} \dfrac{\partial\phi}{\partial t} + \mathbf{u}\cdot\nabla\phi = M\Delta\mu, \quad \text{in } \Omega, \\ \mu = -\epsilon\Delta\phi - \dfrac{1}{\epsilon}(\phi - \phi^3), \quad \text{in } \Omega, \\ R\rho\left[\dfrac{\partial\mathbf{u}}{\partial t} + (\mathbf{u}\cdot\nabla)\mathbf{u}\right] = -\nabla p + \nabla\cdot(\eta\nabla\mathbf{u}) + \kappa\mu\nabla\phi, \quad \text{in } \Omega, \\ \nabla\cdot\mathbf{u} = 0, \quad \text{in } \Omega, \end{cases} \tag{2.6}$$

where R is the Reynolds number, $\mathbf{u}$ is the velocity, p is the pressure, ρ is the density and η is the viscosity. The term $\kappa\mu\nabla\phi$ represents the capillary force. We use the relaxational boundary condition for the phase field variable

$$\phi_t + u_\tau\partial_\tau\phi = -\Gamma\left(\epsilon\partial_n\phi - \frac{\sqrt{2}}{6}\pi\cos\theta_s\cos\frac{\pi\phi}{2}\right), \quad \text{on } \partial\Omega. \tag{2.7}$$

The tangent velocity along the solid boundary can be evaluated as

$$\frac{u_\tau^{slip}}{l_s} = -(\partial_n u_\tau + \partial_\tau u_n) + \kappa\left[\left(\epsilon\partial_n\phi - \frac{\sqrt{2}}{6}\pi\cos\theta_s\cos\frac{\pi\phi}{2}\right)\partial_\tau\phi\right]\Big/\eta, \text{ on } \partial\Omega, \tag{2.8}$$

where $u_n = \mathbf{u}\cdot\mathbf{n}$ and $u_\tau = \mathbf{u}\cdot\tau$ is the velocity along the normal and tangent direction of the boundary respectively, where $\mathbf{n} = \{n_x, n_y\}$ and $\tau = \{\tau_x, \tau_y\}$ are the unit normal and tangent vector of the slip boundary. Here l_s represents the slip length. In addition, the following non-penetration boundary conditions are used on the solid boundary

$$u_n = 0, \quad \partial_n\mu = 0, \quad \text{on } \partial\Omega. \tag{2.9}$$

We use a convex splitting finite element scheme to solve the above system numerically. The details of the numerical scheme is given in [27]. The scheme is linear and unconditionally stable and is capable of simulating problems on complex

geometries. In the following sections, we study the Cassie and Wenzel states transition and the phenomena of contact angle hysteresis of droplet spreading on topologically rough surfaces. We only consider two dimensional situations here, and we assume the size of droplet is sufficiently small so that gravity can be neglected.

3 Cassie and Wenzel states transition

We consider a two dimensional droplet suspended on a regular array of posts with width b, height h and distance d between each other as shown in Figure 1. We will study the conditions under which the Cassie or Wenzel state can occur and the transition between the two states. It is easy to see that if the surface of the substrate is hydrophilic, the droplet will always collapse into Wenzel state. Therefore we will only consider the case that the substrate is hydrophobic, which means that the equilibrium Young's angle θ_s satisfies $\theta_s > 90°$.

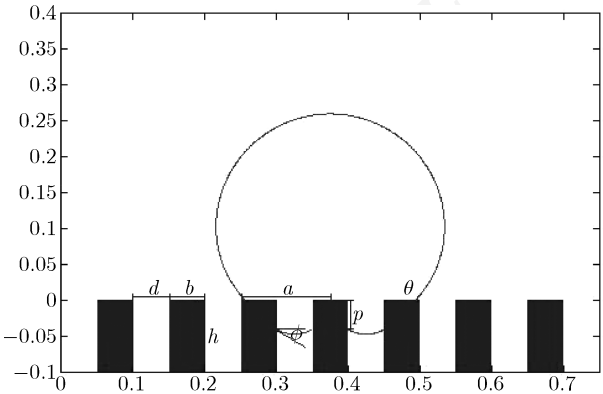

Figure 1: Schematic diagram of a droplet suspended on an array of pillars.

Above the posts, the droplet can form a circular cap with contact angle θ and droplet cross-sectional area S. Here for simplicity, we assume that the contact line of the droplet is pinned at the edges of the outer pillars. Then θ is not necessarily to be its equilibrium contact angle θ_s because of the contact angle hysteresis. It can vary between the advancing contact angle 180° and receding contact angle θ_s. Given pinning, we see that the base radius a is fixed and takes values of

$$a = \left(m + \frac{1}{2}\right) b + md = R \sin\theta, \tag{3.1}$$

where $2m + 1 = 1, 2, 3, \ldots$ is the number of posts beneath the drop, and R is the radius of the cap.

In the bottom region of the droplet, if it has impaled into the posts with penetration depth p, each curved interface is part of a circle with circumferential angle $\varphi = \theta_s - 90°$. As a consequence, each of the impaled part is modeled as a rectangular with width d and height p plus the circular part. The total area of the two dimensional droplet is fixed to be

$$S = a^2\frac{\theta - \sin\theta\ \cos\theta}{\sin^2\theta} + 2mdp + \frac{2md^2}{4}\frac{\varphi - \sin\varphi\ \cos\varphi}{\sin^2\varphi}. \tag{3.2}$$

We are interested in the dependence of the droplet free energy on penetration depth p with fixed area constraint condition (3.2). Firstly, we assume that the droplet does not touch the bottom of posts, i.e., $p < h$. Ignoring a constant, the lengths of liquid-vapor, solid-liquid and solid-vapor interface are

$$C_{LV} = \frac{2a\theta}{\sin\theta} + \frac{2md\varphi}{\sin\varphi}, \quad C_{SL} = 4mp, \quad C_{SV} = 4m(h-p),$$

respectively. Hence the total surface free energy is given by

$$\begin{aligned} f(p) &= \gamma_{LV}C_{LV} + \gamma_{SL}C_{SL} + \gamma_{SV}C_{SV} \\ &= \gamma_{LV}\left(\frac{2a\theta}{\sin\theta} + \frac{2md\varphi}{\sin\varphi} - 4mp\cos\theta_s\right) + 4\gamma_{SV}mh, \end{aligned} \tag{3.3}$$

where θ is an implicit function of p via the fixed droplet area condition (3.2). Here we have neglected the constant contributions to $f(p)$. By taking the derivative of f, we can get that

$$\frac{df}{dp} = \gamma_{LV}\left[2a\frac{d}{dp}\left(\frac{\theta}{\sin\theta}\right) - 4m\cos\theta_s\right] = \gamma_{LV}\left(2a\frac{\sin\theta - \theta\cos\theta}{\sin^2\theta}\frac{d\theta}{dp} - 4m\cos\theta_s\right).$$

The formula of $\frac{d\theta}{dp}$ can be obtained by using the constraint of fixed droplet area (3.2), which gives

$$\frac{d\theta}{dp} = -\frac{md\ \sin^3\theta}{a^2(\sin\theta - \theta\cos\theta)}. \tag{3.4}$$

Combining the above two equations, we have

$$\frac{df}{dp} = \gamma_{LV}\left(-\frac{2md}{a}\sin\theta - 4m\cos\theta_s\right), \tag{3.5}$$

where the contact angle $\theta \in (\theta_s,\ 180^\circ)$. It is easy to see from (3.4) that θ is decreasing in p. Therefore the right hand side of (3.5), $-\frac{2md}{a}\sin\theta - 4m\cos\theta_s$ is a decreasing function in p.

Consider the relation of the free energy to the penetration depth by the formulation (3.5). There is a critical value $\theta_{s,c} = 180^\circ - \arcsin(\frac{2a}{\sqrt{4a^2+d^2}})$ at which $-\frac{2md}{a}\sin\theta_{s,c} - 4m\cos\theta_{s,c} = 0$. By the monotonicity of $\sin\theta$ and $\cos\theta$ in the interval $(90^\circ,\ 180^\circ)$, it is greater than the critical value $\theta_{s,c}$.

From (3.5), we have

$$\frac{df}{dp} = \gamma_{LV}\left(-\frac{2md}{a}\sin\theta - 4m\cos\theta_s\right) \geq \gamma_{LV}\left(-\frac{2md}{a}\sin\theta_s - 4m\cos\theta_s\right). \tag{3.6}$$

The sign of the right hand side determines the behavior of $f(p)$. Let $\theta_{s,c}$ be a critical value such that $(-\frac{2md}{a}\sin\theta_{s,c} - 4m\cos\theta_{s,c}) = 0$, which gives $\theta_{s,c} = 180^\circ - \arcsin(\frac{2a}{\sqrt{4a^2+d^2}})$. It is easy to see that, if the equilibrium contact angle $\theta_s > \theta_{s,c}$, then

$$\frac{df}{dp} \geq \gamma_{LV}\left(-\frac{2md}{a}\sin\theta_s - 4m\cos\theta_s\right) \geq \gamma_{LV}\left(-\frac{2md}{a}\sin\theta_{s,c} - 4m\cos\theta_{s,c}\right) = 0. \tag{3.7}$$

On the other hand, if $\theta_s < \theta_{s,c}$, then $\frac{df}{dp}$ may become negative (depending on the drop size) in which case the drop starts to penetrate the posts and θ gets smaller. Therefore once $\frac{df}{dp}$ becomes negative it will always be negative. The drop will collapse into the Wenzel state. The condition for the drop to start collapsing is $\frac{df}{dp}|_{p=0} < 0$. The corresponding critical drop radius is $R_c = -\frac{d}{2\cos\theta_s}$ [11]. As we have shown in Figure 2 (b), when the drop radius $R < R_c$, $\frac{df}{dp}$ is always negative and the drop will automatically collapse to the Wenzel state. When the drop radius $R > R_c$, $\frac{df}{dp}$ will be positive for p small. As p becomes greater, there is a critical penetration depth p_c at which $\frac{df}{dp} = 0$, and $\frac{df}{dp}$ will be negative for $p > p_c$. This means that the drop will attain Cassie state if its initial position satisfies $p < p_c$ and collapse to Wenzel state if $p > p_c$. There is a free energy barrier between the Cassie state and Wenzel state for this case.

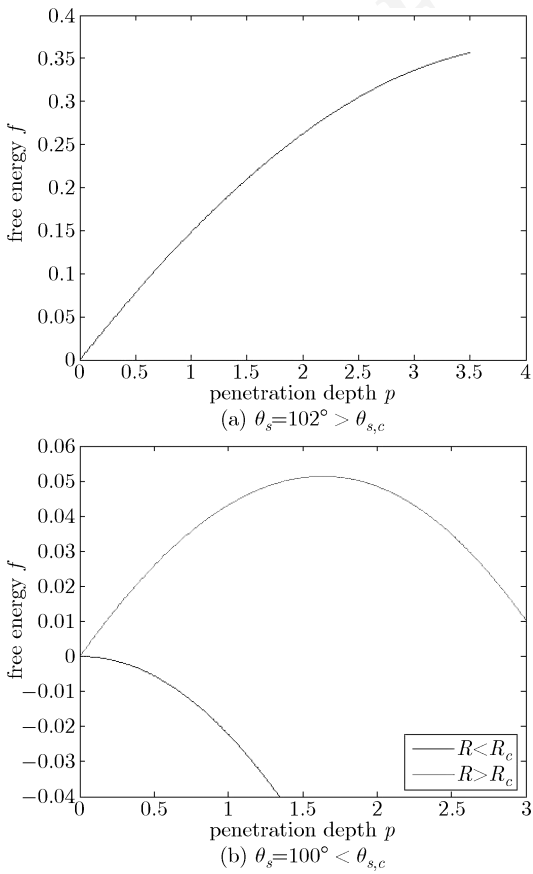

Figure 2: Normalized surface free energy against the penetration depth when (a) $\theta_s > \theta_{s,c}$, and (b) $\theta_s < \theta_{s,c}$.

The above discussion is when the droplet does not touch the bottom substrate of posts. If the lower interface of the droplet is very close to the bottom, then the final reduction in free energy due to the Wenzel transition will be

$$\Delta f = C_{bott}[\gamma_{SL} - (\gamma_{LV} + \gamma_{SV})] = -C_{bott}\gamma_{LV}(1 + \cos\theta_s) \ \leq \ 0, \tag{3.8}$$

where C_{bott} is the bottom length of the posts beneath the droplet, and thus the Wenzel state is always stable.

Now we carry out numerical simulations using the phase field model with GNBC and compare the numerical results with the analytical results above. Guided by the behavior of the free energy curves, we use the droplet of different equilibrium contact angles, radiuses and initial positions, and simulate the behavior of the droplet as it settles into the equilibrium state. Here we use $a = 0.125$ and $b = d = 0.05$. Then the critical equilibrium contact angle $\theta_{s,c} = 101.31°$. For the equilibrium contact angle $\theta_s = 98° < \theta_{s,c}$, the corresponding critical droplet radius $R_c = 0.1796$. Firstly we take the droplet radius $R = 0.2 > R_c$, there should be an energy barrier between the Cassie and Wenzel states as seen in Figure 3

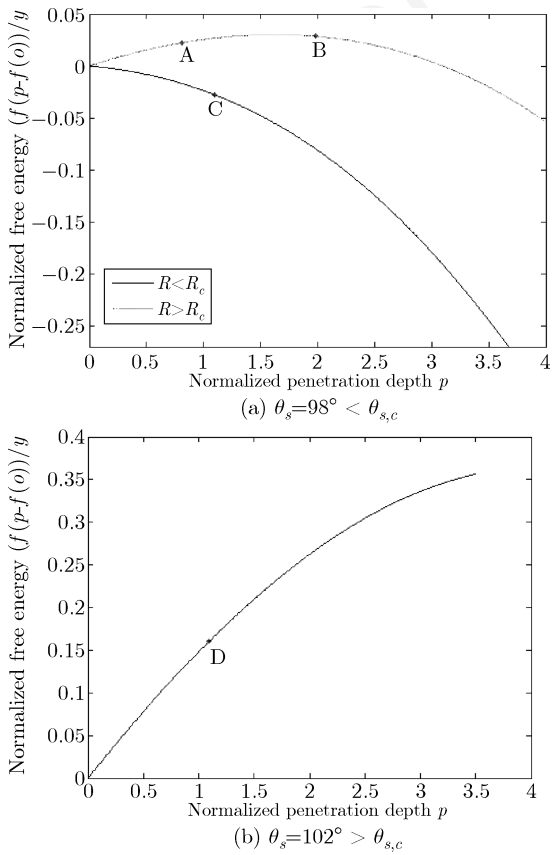

Figure 3: Normalized surface free energy against the penetration depth when (a) $\theta_s < \theta_{s,c}$, and (b) $\theta_s > \theta_{s,c}$.

(a).Our numerical results also demonstrate this. Figure 4 (a) and (b) show that if we put the droplet at position A, the droplet will retreat to the Cassie's state, and if we put the droplet at position B, then the droplet will collapse to the Wenzel's state. Next, we take the droplet radius $R = 0.175 < R_c$. By the theoretical result, the free energy will decrease as the penetration depth p gets greater, and Figure 4 (c) shows that the droplet will collapse to the Wenzel's state if we put the droplet at position C.

Taking the equilibrium contact angle $\theta_s = 102^\circ > \theta_{s,c}$, theoretically the Cassie's state should always be stable because the free energy increases with the penetration depth p. Figure 4 (d) shows that the droplet retreats to Cassie's state with the same conditions as (c) except that the equilibrium contact angle is changed to be 102°. From the figures above, we can see that the numerical simulation results agree quantitatively well with the predictions of the free energy curves. We choose the interface thickness $\epsilon = 0.01$ in all our numerical simulations.

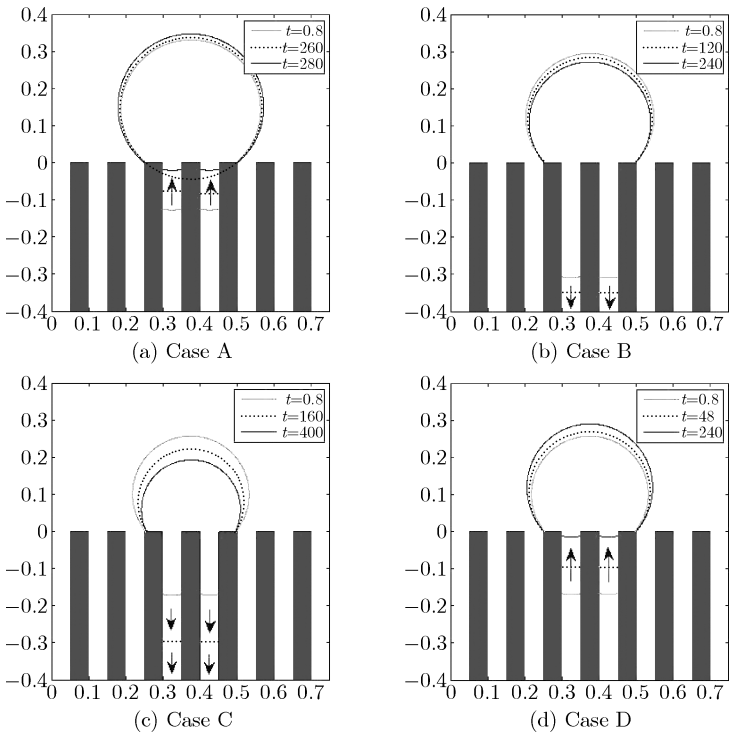

(a) Case A (b) Case B

(c) Case C (d) Case D

Figure 4: Numerical results of droplet with different contact angles, radiuses and initial positions corresponding to A, B, C and D in Figure 3, respectively.

4 Droplet spreading on superhydrophobic surface

The phenomena of roughness induced superhydrophobicity is frequently seen in nature and has been demonstrated to be useful in many applications, e.g., the

lotus effect, water-resistant material and so on. When surfaces with an intrinsic hydrophobic contact angle are covered with microscale posts, the apparent contact angle can be greatly increased, and the droplet can lie in a suspended state on top of the posts, i.e., the Cassie's state. Most frequently, the apparent contact angle is given by equation (1.2), which is known as the Cassie-Baxter's equation. The contact angle hysteresis on these surfaces is relatively small and droplets can easily roll off. It is usually known that the contact angle hysteresis is related to the chemically patterns and topologically roughnesses of the substrate. Here we will study the contact angle hysteresis on roughness induced superhydrophobic surfaces.

Similar to Section 3.1, consider a two dimensional droplet suspended on a regular array of posts with width b, height h and distance d between each other. The base radius of the droplet is a. The solid substrate is hydrophobic. In this section, we assume that the droplet is always suspended on the posts of substrate.

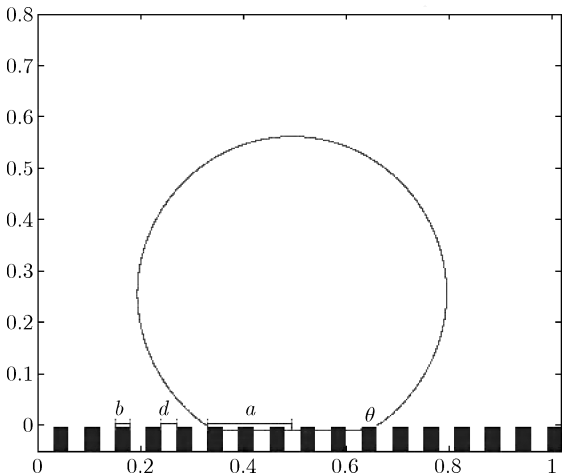

Figure 5: Schematic diagram of a droplet suspended on an array of pillars.

Above the posts, the droplet can form a circular cap with contact angle θ and droplet area S. If the contact line of the droplet is pinned at the edges of posts, the contact angle θ is not necessarily to be its equilibrium contact angle θ_s because of the contact angle hysteresis. It can vary between the advancing and receding contact angles. By the assumptions above, there is no penetration into the posts, the bottom base of the droplet can be regarded to be flat. This is reasonable when the droplet is much larger than the size of posts.

As in Section 3.1, the shape of the droplet is a circular cap with contact angle θ. Obviously, the total area of the droplet can be written as

$$S = a^2 \, \frac{\theta - \sin\theta\cos\theta}{\sin^2\theta}. \tag{4.1}$$

Because the contact point can only be on the solid surface, the base radius a should only take values of $[\max\{(m-\frac{1}{2})b+md, 0\}, \ (m+\frac{1}{2})b+md]$, where $2m+1 = 1, 2, 3, ...$

is the number of posts beneath the droplet. We are interested in the dependence of surface free energy on the contact angle θ with fixed area constraint condition (4.1). Ignoring a constant and using the Young's equation (1.1), the surface free energy is given by

$$f(\theta) = \gamma_{LV}\left[2a\frac{\theta}{\sin\theta} + 2md - 2(a-md)\cos\theta_s\right], \tag{4.2}$$

where the base radius a is a function of θ via the droplet area constraint condition (4.1),

$$a = \sin\theta\sqrt{\frac{S}{\theta - \sin\theta\cos\theta}}. \tag{4.3}$$

Thus, the relation of free energy function f to the contact angle θ is

$$f(\theta)=\gamma_{LV}\left[2\theta\sqrt{\frac{S}{\theta-\sin\theta\cos\theta}}+2md(1+\cos\theta_s)-2\cos\theta_s\sin\theta\sqrt{\frac{S}{\theta-\sin\theta\cos\theta}}\right], \tag{4.4}$$

where θ should also take piecewise values by (4.1) for fixed droplet size S. By simple calculations, we can get that in each segment

$$\frac{df}{d\theta} = 2\gamma_{LV}\sqrt{S}\frac{(\theta\cos\theta - \sin\theta)(\cos\theta - \cos\theta_s)}{(\theta - \sin\theta\cos\theta)^{\frac{3}{2}}}. \tag{4.5}$$

Obviously, $\frac{df}{d\theta} > 0$ if $\theta > \theta_s$, and $\frac{df}{d\theta} < 0$ if $\theta < \theta_s$, which means that the energy curve is piecewise increasing when $\theta > \theta_s$, and piecewise decreasing when $\theta < \theta_s$.

Let λ be the fraction of solid-liquid interface below the droplet. For fixed λ, if we let the roughness sizes b and d approach to zero, the solid surface can be seen as a perfectly homogenized material. The base below the droplet includes the solid-liquid interface with length of $2a\lambda$ and the liquid-vapor interface with length of $2a(1-\lambda)$. Thus the surface free energy can be written as

$$f(\theta) = 2\gamma_{LV}\sin\theta\sqrt{\frac{S}{\theta - \sin\theta\cos\theta}}\left\{\frac{\theta}{\sin\theta} - [\lambda\cos\theta_s - (1-\lambda)]\right\}. \tag{4.6}$$

In this case, by taking the derivative of f, we can get that

$$\frac{df}{d\theta} = 2\gamma_{LV}\sqrt{S}\,\frac{\theta\cos\theta - \sin\theta}{(\theta - \sin\theta\cos\theta)^{\frac{3}{2}}}\,\{\cos\theta - [\lambda\cos\theta_s - (1-\lambda)]\}. \tag{4.7}$$

Let $\frac{df}{d\theta} = 0$, we have $\cos\theta = \lambda\cos\theta_s - (1-\lambda)$, which is the Cassie-Baxter's equation. This implies that the Cassie-Baxter's angle is the contact angle corresponding to the free energy minimum when the roughness size is much smaller than the size of droplet.

We now compute free energy curves for different roughness sizes. We keep the roughness fraction λ fixed ($\lambda = 0.5$ here) and use three pairs of different roughness parameters $b = d = 0.05$, 0.03 and 0.02 respectively. The droplet size S is fixed to be 0.2827 and the equilibrium contact angle $\theta_s = 100°$. Figure 6 shows the

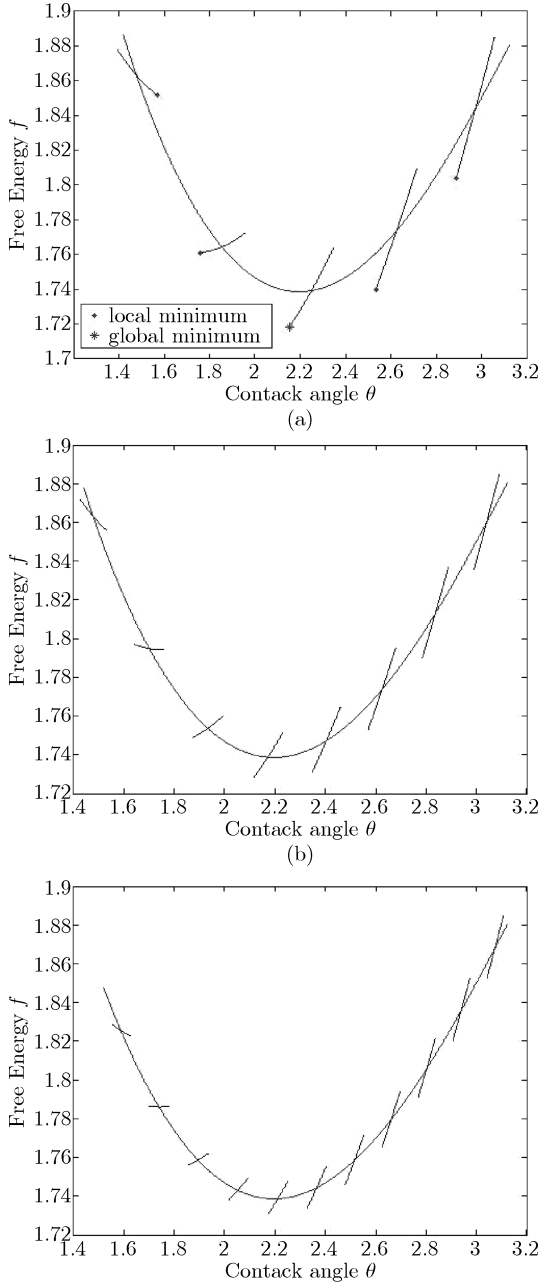

Figure 6: Surface free energy f against the contact angle θ when the roughness size (a) $b = d = 0.05$, (b) $b = d = 0.03$ and (c) $b = d = 0.02$. The continuous line is the energy curve of (4.6), while the discontinuous line is the energy curve of (4.4). The energy curve for (4.4) is piecewise continuous because the base radius a could only take piecewise values.

free energy curves via the contact angle θ when $b = d = 0.05$, 0.03 and 0.02 respectively. The continuous line is the energy curve of formulation (4.6). We can see that when the roughness size becomes smaller, the discontinuous energy curves get closer to the continuous curve. There are multiple local minimums (metastable states) and energy barriers for the discontinuous energy curve. The strength of the energy barrier gets weaker away from the global minimum. The energy barrier also gets weaker when the roughness size becomes smaller. The contact angles corresponding to the global energy minimum are 123.3°, 121.0° and 124.4° respectively, and all close to the Cassie-Baxter's angle is 125.9°.

To simulate the droplet spreading using the phase field model, we choose $\epsilon = 0.01$, which is comparable to the sizes of roughness. This will cause the contact line to feel the neighboring posts and hence can overcome some energy barriers by jumping across to it when the height of the barrier is low. We remark that it is reasonable because there are energy vibrations and thermal fluctuations in real systems, which will make the droplet overcome some energy barriers.

Since we are interested in the equilibrium state of the droplet which may depend on the initial position, we take the initial contact angles of the droplet to be 180° and 90° respectively. If the initial contact angle is 180°, the droplet will advance to its equilibrium state, and if the initial contact angle is 90°, it will recede to the equilibrium state.

In both cases, the phenomena of stick-slip is observed by our numerical simulations. The contact line is pinned at a position for some time and can jump to the neighboring post if the energy barrier is weak enough, accompanied by a sudden decrease or increase in the contact angle and the droplet base radius. The process then repeats until it reaches its equilibrium state.

Figure 7 shows the configurations of droplet advancing to its equilibrium state with decreasing roughness sizes $b = d = 0.05$, 0.03 and 0.02. The droplet reaches its equilibrium state at the contact angles of 145.2°, 147.3° and 135.9°, respectively. As we can see, as the size of the roughness decreases (and the size of the barrier becomes weaker), the interface can overcome more energy barriers and reaches an equilibrium state which is closer to the Cassie-Baxter state.

Similarly, the results for the receding case are shown in Figure 9 and Figure 10. When the droplet recedes to its equilibrium state, the equilibrium contact angles are 100.7°, 107.5° and 124.4° for the roughness size $b = d = 0.05$, 0.03 and 0.02 respectively.

5 Conclusions

In this paper, we have first investigated the possible Cassie and Wenzel states transition on rough hydrophobic substrates in two dimensions. By considering the free energy of the system, we find that the meta-stability of different wetting states would depend on the equilibrium contact angle, the droplet size and its initial position. There is a critical value for the static contact angle. For contact angle greater than the critical value, the droplet will always be static in Cassie state. When the contact angle is smaller than the critical value, the state of droplet is

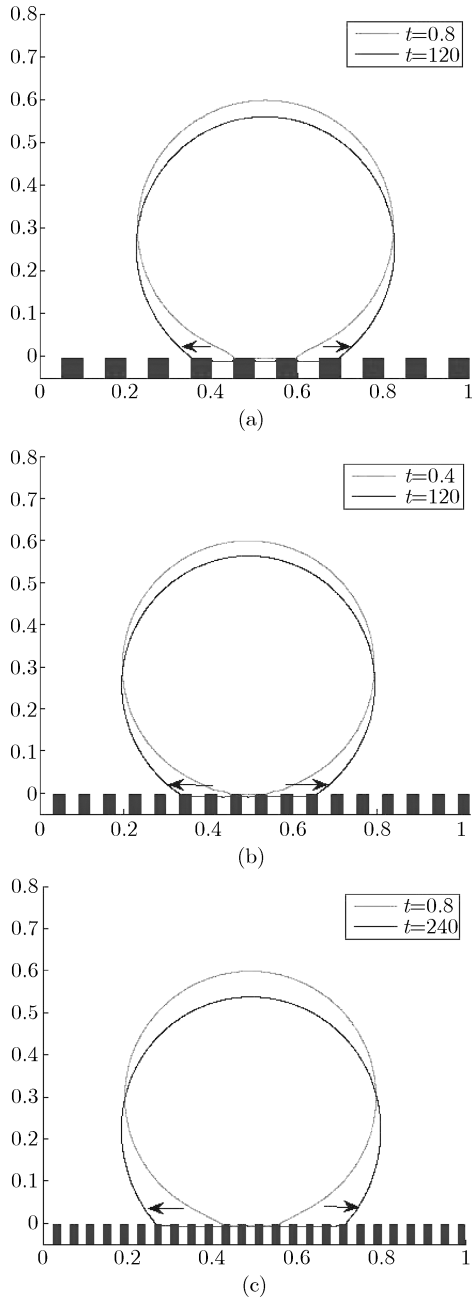

Figure 7: Advancing evolution with time when the roughness size (a) $b = d = 0.05$, (b) $b = d = 0.03$ and (c) $b = d = 0.02$. The black line is the equilibrium configuration of the contour.

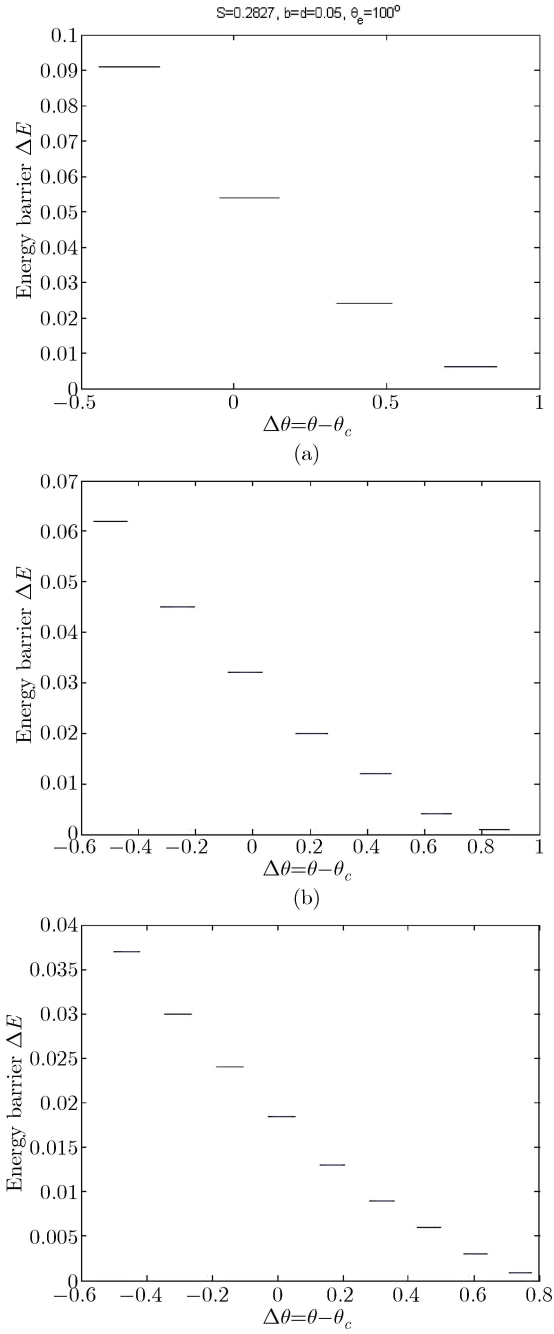

Figure 8: Energy barriers in advancing process when the roughness size (a) $b = d = 0.05$, (b) $b = d = 0.03$ and (c) $b = d = 0.02$. The number of barriers that can overcome are one, two, and four respectively. Here θ_c is the Cassie-Baxter's angle.

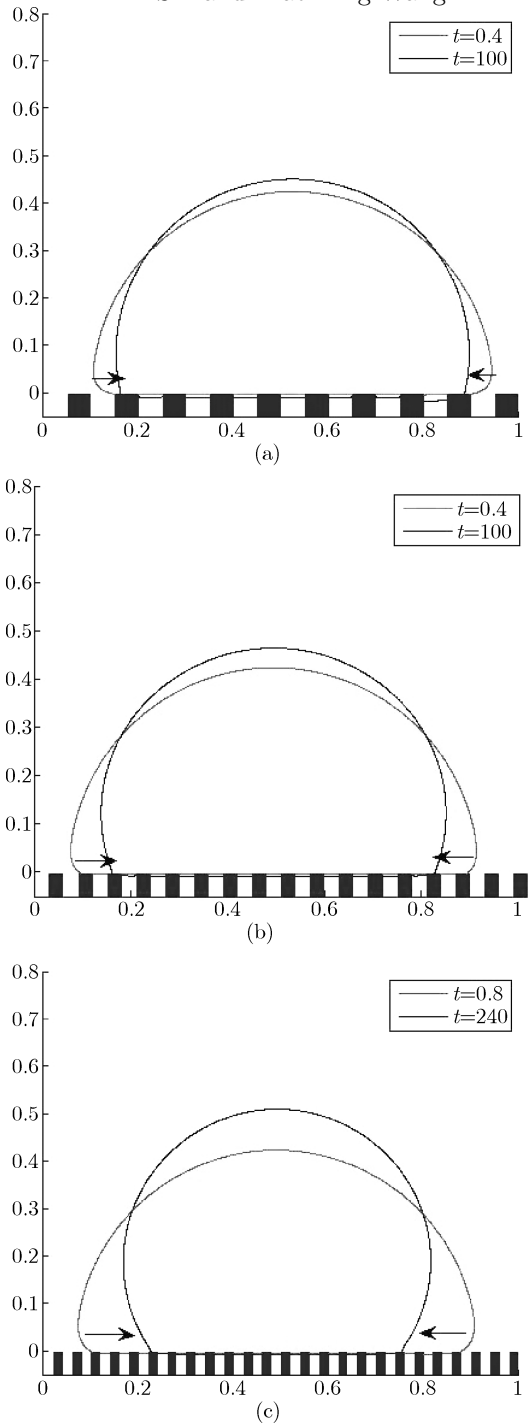

Figure 9: Receding evolution with time when the roughness size (a) $b = d = 0.05$, (b) $b = d = 0.03$ and (c) $b = d = 0.02$. The black line is also the equilibrium configuration of the contour.

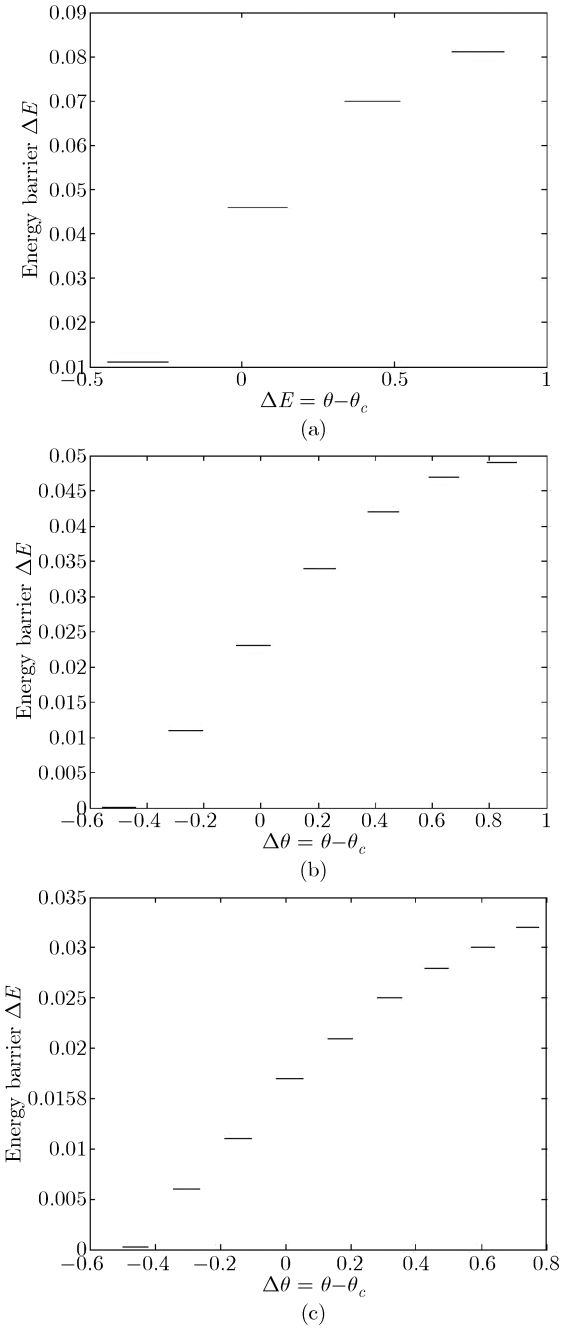

Figure 10: Energy barriers in receding process when the roughness size (a) $b = d = 0.05$, (b) $b = d = 0.03$ and (c) $b = d = 0.02$. The number of barriers that can overcome are zero, one and two respectively. θ_c is also the Cassie-Baxter's angle.

determined by the droplet size and its initial position. Numerical simulations of

our phase field model agrees quantitatively well with the analytical results. We have also studied the quasi-static spreading of the droplet on superhydrophobic surfaces, where the droplet is suspended in Cassie state on substrates with different sizes. From analysis of the free energy landscape, we find that the Cassie-Baxter's contact angle is the most stable contact angle when the droplet size is much larger than the size of roughness. There are multiple local energy minimums and one global energy minimum for the free energy of the system, which can reveal the mechanism of stick-slip phenomena. For the phase field model, the diffusive interface thickness can play the role of energy vibration, which allows the droplet to overcome some energy barriers. When the size of roughness becomes smaller, the stick-slip phenomena becomes weaker and the apparent contact angle will get closer to the Cassie-Baxter's contact angle.

Acknowledgement. This work is supported in part by the Hong Kong RGC grants GRF-HKUST 605513, 605311 and NNSF of China grant 91230102.

References

[1] Tiezheng Qian, Xiao-Ping Wang, Ping Sheng, Molecular scale contact line hydrodynamics of immiscible flows, Phys. Rev. E 68 (2003), 016306.

[2] Xiao-Ping Wang, Tiezheng Qian, Ping Sheng, Moving contact line on chemically patterned surfaces, J. Fluid Mech. 605 (2008), 59–78.

[3] Tiezheng Qian, Xiao-Ping Wang, Ping Sheng, Molecular hydrodynamics of the moving contact line in two-phase immiscible flows, Commun. Comput. Phys. 1 (2006), 1–52.

[4] Tiezheng Qian, Xiao-Ping Wang, Ping Sheng, A variational approach to the moving contact line hydrodynamics, J. Fluid Mech. 564 (2006), 333–306.

[5] Yana Di, Xiao-Ping Wang, Precursor simulations in spreading using a multi-mesh adaptive finite elment method, J. Comput. Phys. 228 (2009), 1380–1390.

[6] Qiaolin He, R. Glowinski, Xiao-Ping Wang, A least square/finite element method for the numerical solution of the Navier-Stokes-Cahn-Hilliard system modeling the motion of the contact line, J. Comput. Phys. 230 (2011), 4991–5009.

[7] Min Gao, Xiao-Ping Wang, A gradient stable scheme for a phase field model for the moving contact line problem, J. Comput. Phys. 231 (2012), 1372–1386.

[8] Xiongping Luo, Xiao-Ping Wang, Tiezheng Qian, Ping Sheng, Moving contact line over undulating surfaces, Solid. Stat. Commun. 139 (2006), 623–629.

[9] Pengtao Yue, James J. Feng, Chun Liu, Jie Shen, A diffuse-interface method for simulating two-phase flows of complex fluids, J. Fluid Mech. 515 (2004), 293–317.

[10] V. Girault, P. Raviart, Finite Element Method for Navier-Stokes Equations: theory and Algorithms, Springer-Verlag, Berlin, Heidlberg, New York, 1981.

[11] H. Kusumaatmaja, M. L. Blow, A. Dupuis, J. M. Yeomans, The collapse transition on superhydrophobic surfaces, Europhys. Lett. 81 (2008), 36003.

[12] H. Kusummaatmaja, J. M. Yeomans, Modeling contact angle hysteresis on chemically patterned and superhydrophobic surfaces, Langmuir 23 (2007), 6019–6032.

[13] B. M. Mognetti, J. M. Yeomans, Modeling receding contact lines on superhydrophobic surfaces, Langmuir 26 (2010), 18162–18168.

[14] A. Dupuis, J. M. Yeomans, Modeling droplets on superhydrophobic surfaces: equilibrium states and transitions, Langmuir 21 (2005), 2624–2629.

[15] Neelesh A. Patankar, Transition between superhydrophobic states on rough surfaces, Langmuir 20 (2004), 7097–7102.

[16] Xianmin Xu, Xiao-Ping Wang, Derivation of Wenzel's and Cassies's equations from a phase field model for two phase flow on rough surface, SIAM J. Appl. Math. 70 (2010), 2929–2941.

[17] Xianmin Xu, Xiao-Ping Wang, Analysis of wetting and contact angle hysteresis on chemically patterned surfaces, SIAM J. Appl. Math. 71(2011), 1753–1779.

[18] Markus Gross, Fathollah Varnik, Dierk Raabe, Ingo Steinbach, Small droplets on superhydrophobic substrates, Phys. Rev. E 81 (2010), 051606.

[19] Livio Fedeli, Alessandro Turco, Antonio DeSimone, Metastable equilibria of capillary drops on solid surfaces: a phase field approach, Continuum Mech. Thermodyn. 23 (2011), 453–471.

[20] Alessandro Turco, Francois Alouges, Antonio DeSimone, Wetting on rough surfaces and contact angle hyeteresis: numerical experiments based on a phase field model, ESIAM: M2AN 43 (2009), 1027–1044.

[21] Neelesh A. Patankar, Hysteresis with regards to Cassie and Wenzel states on superhydrophobic surfaces, Langmuir 26 (2010), 7498–7503.

[22] Xueyun Zhang, Yongli Mi, Dynamics of a stick-jump contact line of water drops on a strip surface, Langmuir 25 (2009), 3212–3218.

[23] Abraham Marmur, Wetting on hydrophobic rough surfaces: to be heterogeneous or not to be?, Langmuir 19 (2003), 8343–8348.

[24] Abraham Marmur, Eyal Bittoun, When Wenzel and Cassie are right: reconciling local and global considerations, Langmuir 25 (2009), 1277–1281.

[25] M. A. Rodriguez-Valverde, F. J. Montes Ruiz-Cabello, M. A. Cabrerizo-Vilchez, Wetting on axially-patterned heterogeneous surfaces, Advances in Colloid and Interface Science 138(2008), 84–100.

[26] J. Long, P. Chen, On the role of energy barriers in determining contact angle hysteresis, Advances in Colloid and Interface Science 127(2006), 55–66.

[27] Kai Bao, Yi Shi, Shuyu Sun, Xiao-Ping Wang, A finite element method for the numerical solution of the coupled Cahn-Hilliard and Navier-Stokes system for moving contact line problems, J. Comput. Phys. 231(2012), 8083–8099.

[28] Weiqing Ren, Weinan E, Contact line dynamics on heterogeneous surfaces, Phys. Fluids, 23 (2011), 072103.

[29] C. Ishino, K. Okumura, D. Quéré, Wetting transitions on rough surfaces, Europhys. Lett. 68 (2008), 419–425.

[30] Vlado A. Lubarda, Kurt A. Talke, Analysis of the equilibrium droplet shape based on an ellipsoidal droplet model, Langmuir 27 (2011), 10705–10713.

Institute of Applied Physics and Computational Mathematics
Beijing 100094, China
E-mail address: shiyi@iapcm.ac.cn

Department of Mathematics, The Hong Kong University of Science and Technology
Clear Water Bay, Kowloon, Hong Kong, China
E-mail address: mawang@ust.hk